Effects of Ion Binding on the Backbone Dynamics of Calbindin D_{9k} Determined by ^{15}N NMR Relaxation†

Mikael Akke,‡,§ Nicholas J. Skelton,‡,∥ Johan Kördel,‡,⊥ Arthur G. Palmer, III,*,# and Walter J. Chazin*,‡

Department of Molecular Biology, The Scripps Research Institute, La Jolla, California 92037, and Department of Biochemistry and Molecular Biophysics, Columbia University, New York, New York 10032

Received February 9, 1993; Revised Manuscript Received June 14, 1993®

ABSTRACT: The backbone dynamics of apo- and $(Cd^{2+})_1$-calbindin D_{9k} have been characterized by ^{15}N nuclear magnetic resonance spectroscopy. Spin–lattice and spin–spin relaxation rate constants and steady-state $\{^1H\}$–^{15}N nuclear Overhauser effects were measured at a magnetic field strength of 11.74 T by two-dimensional, proton-detected heteronuclear NMR experiments using ^{15}N-enriched samples. The relaxation parameters were analyzed using a model-free formalism that characterizes the dynamics of the N–H bond vectors in terms of generalized order parameters and effective correlation times. The data for the apo and $(Cd^{2+})_1$ states were compared to those for the $(Ca^{2+})_2$ state [Kördel, J., Skelton, N. J., Akke, M., Palmer, A. G., & Chazin, W. J. (1992) *Biochemistry 31*, 4856–4866] to ascertain the effects of ion ligation on the backbone dynamics of calbindin D_{9k}. The two binding loops respond differently to ligation by metal ions: high-frequency (10^9–10^{12} s^{-1}) fluctuations of the N-terminal ion-binding loop are not affected by ion binding, whereas residues G57, D58, G59, and E60 in the C-terminal ion-binding loop have significantly lower order parameters in the apo state than in the metal-bound states. The dynamical responses of the four helices to binding of ions are much smaller than that for the C-terminal binding loop, with the strongest effect on helix III, which is located between the linker loop and binding site II. Significant fluctuations on slower time scales also were detected in the unoccupied N-terminal ion-binding loop of the apo and $(Cd^{2+})_1$ states; the apparent rates were greater for the $(Cd^{2+})_1$ state. These results on the dynamical response to ion binding in calbindin D_{9k} provide insights into the molecular details of the binding process and qualitative evidence for entropic contributions to the cooperative phenomenon of calcium binding for the pathway in which the ion binds first in the C-terminal site.

Calbindin D_{9k} is a small protein of 75 residues that belongs to the S-100 subgroup of the calmodulin superfamily of intracellular calcium-binding proteins (Heizmann & Hunziker, 1991). This family of proteins exhibits a wide diversity of functions ranging from maintaining intracellular Ca^{2+} levels to mediating specific cellular responses. Calbindin D_{9k} is involved in intracellular buffering of calcium ions and/or uptake of calcium ions from the intestinal brush border membrane and transport to the basolateral membrane [reviewed by Staun (1991) and Christakos et al. (1989)]. Calcium-dependent interactions between calbindin D_{9k} and the calmodulin-binding domain of the plasma membrane calcium pump (Ca^{2+}-ATPase) have been observed *in vitro* (James et al., 1991).

The calmodulin superfamily is characterized by a common helix–loop–helix structural motif in the calcium-binding sites, termed the EF-hand (Kretsinger, 1972). The basic functional unit for the majority of these proteins is a pair of EF-hands (Seamon & Kretsinger, 1983), and cooperative binding of calcium ions has been established in several cases. Calbindin D_{9k} contains a single pair of EF-hands with the characteristic topology of the S-100 proteins: the N-terminal EF-hand has a variant ion-binding loop with 14 residues, as opposed to the 12 residues of a typical calmodulin-like EF-hand. The protein binds two calcium ions with high affinity and positive cooperativity (Linse et al., 1987, 1991).

In order to assess the structural and dynamical changes that accompany the binding of calcium ions to calbindin D_{9k} and to determine the molecular basis for the observed cooperativity, research in this laboratory has involved NMR[1] spectroscopy to study the apo and calcium-saturated $[(Ca^{2+})_2]$ states, as well as the half-saturated states with an ion bound in the N-terminal site I $[(Ca^{2+})_1^I]$ or the C-terminal site II $[(Ca^{2+})_1^{II}]$. Wild-type calbindin D_{9k} is present in two isoforms under equilibrium conditions in solution due to *cis–trans* isomerization of the G42–P43 peptide bond in the flexible linker loop between the two EF-hands (Chazin et al., 1989a). The P43G mutant exists in a single isoform, thereby elimi-

† This work was supported by the National Institutes of Health (Grant GM 40120 to W.J.C.), The American Cancer Society (fellowship JFRA294 to W.J.C.), the Swedish Natural Science Research Council (graduate fellowships to M.A. and J.K.), and the Royal Swedish Academy of Sciences (scholarship to M.A.).

* Author to whom correspondence should be addressed.

‡ The Scripps Research Institute.

§ Permanent address: Department of Physical Chemistry 2, University of Lund, S-221 00 Lund, Sweden.

∥ Present address: Department of Protein Engineering, Genentech, Inc., South San Francisco, CA 94080.

⊥ Present address: Department of Biological Chemistry and Molecular Pharmacology, Harvard Medical School, Boston, MA 02115.

Columbia University.

® Abstract published in *Advance ACS Abstracts*, August 15, 1993.

[1] Abbreviations: ANOVA, analysis of variance; $(Ca^{2+})_1^I$ state, calbindin D_{9k} with one calcium ion bound to site I; $(Ca^{2+})_1^{II}$ state, calbindin D_{9k} with one calcium ion bound to site II; $(Ca^{2+})_2$ state, calbindin D_{9k} with a calcium ion bound in each site; $(Cd^{2+})_1$ state, calbindin D_{9k} with one cadmium ion bound to site II; $(Cd^{2+})_2$ state, calbindin D_{9k} with a cadmium ion bound in each site; CPMG, Carr–Purcell–Meiboom–Gill; CSA, chemical shift anisotropy; FID, free induction decay; INEPT, insensitive nuclei enhanced by polarization transfer; NMR, nuclear magnetic resonance; NOE, nuclear Overhauser effect; P43G, recombinant bovine calbindin D_{9k} mutant with proline 43 substituted by glycine; R_1, spin–lattice or longitudinal relaxation rate constant; R_2, spin–spin or transverse relaxation rate constant; RMS, root-mean-square; SSE, sum-squared-error; TPPI, time-proportional phase incrementation.

0006-2960/93/0432-9832$04.00/0

nating problems associated with the presence of two sets of resonances in the NMR spectra. A wide-ranging and detailed comparative ^1H NMR analysis revealed only minimal differences in the structural and dynamical properties between the P43G mutant and the two isoforms of the wild-type protein (Kördel et al., 1990). Furthermore, the calcium-binding properties of the P43G mutant are very similar to those of the wild-type, and positive cooperativity is clearly retained (Kördel et al., 1990).[2] All current studies are carried out on the P43G mutant, and references herein to calbindin D_{9k} denote this mutant unless otherwise indicated. Due to the cooperativity in calcium binding, neither the $(Ca^{2+})_1^I$ nor $(Ca^{2+})_1^{II}$ state is sufficiently populated under equilibrium conditions for study by NMR. This obstacle has been circumvented by two different approaches: the $(Cd^{2+})_1$ state has been used as a model for the $(Ca^{2+})_1^{II}$ state (Akke et al., 1991), and recently the $(Ca^{2+})_1$ state of the E65Q–P43M double mutant has been used as a model for the $(Ca^{2+})_1^I$ state (Carlström & Chazin, 1993). Both of these model systems bind the respective ions sequentially and thereby allow detailed characterization of the respective half-saturated states by NMR.

The three-dimensional structure of calbindin D_{9k} is depicted in Figure 1, showing the organization of the four helices (I–IV), the N-terminal and C-terminal Ca^{2+}-binding loops (loop I and loop II, respectively), and the linker loop. Comparison of high-resolution three-dimensional solution structures of calbindin D_{9k} in the apo (N. J. Skelton, J. Kördel, and W. J. Chazin, unpublished results) and $(Ca^{2+})_2$ states (Akke et al., 1992; Kördel et al., 1993) demonstrates that the conformational differences between the two states are limited. In contrast, a variety of NMR parameters sensitive to the dynamical properties of the proteins, including chemical shifts and amide proton exchange rates, indicate that the flexibility of calbindin D_{9k} is reduced upon ion binding (Skelton et al., 1990, 1992a; Akke et al., 1991). These results have lent considerable support to the hypotheses that intramolecular dynamics are an important factor in the function of calbindin D_{9k} and that changes in dynamic processes in the protein upon Ca^{2+} binding contribute appreciably to cooperativity. However, analyses of chemical shifts and amide proton exchange rates do not rigorously discriminate between the changes in structure and changes in dynamics that accompany the binding of ions. To this end, a series of nuclear magnetic spin relaxation studies has been initiated that report directly on the dynamic consequences of ion binding in calbindin D_{9k}.

The development of proton-detected heteronuclear NMR experiments [reviewed by Bax et al. (1989)] has engendered a number of recent ^{13}C [e.g., Nirmala and Wagner (1988) and Palmer et al. (1991a)] and ^{15}N [e.g., Kay et al. (1989) and Clore et al. (1990a)] relaxation studies of peptides and proteins, including $(Ca^{2+})_2$-calbindin D_{9k} (Kördel et al., 1992) and $(Ca^{2+})_4$-calmodulin (Barbato et al., 1992). The present report describes the backbone dynamics of apo- and $(Cd^{2+})_1$-calbindin D_{9k}, as determined from ^{15}N spin relaxation measurements performed using proton-detected ^{15}N–^1H 2D NMR spectroscopy. Results for the apo and $(Cd^{2+})_1$ states of calbindin D_{9k} are compared to the corresponding results previously obtained for the $(Ca^{2+})_2$ state (Kördel et al., 1992). This comparison between the three states of the protein provides detailed information on the changes in dynamics that result from ion binding and illuminates aspects of the molecular basis for cooperativity in Ca^{2+} binding.

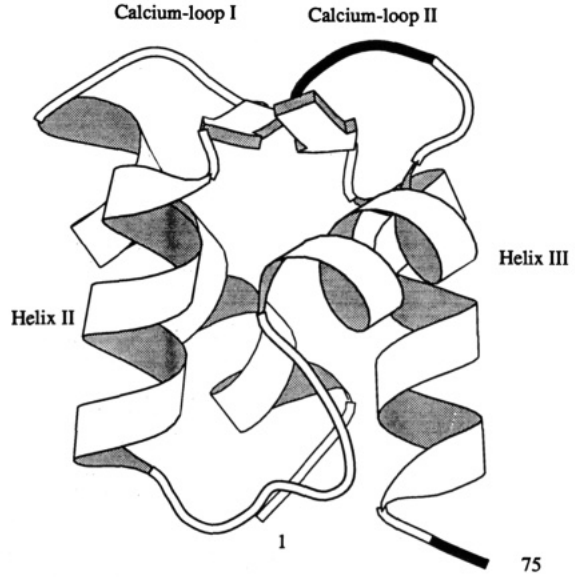

FIGURE 1: Ribbon diagram of the three-dimensional structure of calbindin D_{9k}, in an orientation with the N-terminal (pseudo) EF-hand to the left and the C-terminal EF-hand to the right. Helices I and IV are in the background, while helices II and III, together with the intervening linker loop, are in the foreground. The ion-binding loops are at the top of the figure, with the short β-type interaction between the ion-binding loops depicted by arrows. Individual residues showing significant differences in the value of the generalized order parameter S^2 between the apo and ion-bound states are highlighted (darker shading). Residues G57, D58, G59, and E60 in loop II have lower order parameters in the apo state than in the $(Cd^{2+})_1$ and $(Ca^{2+})_2$ states, while S74 and Q75 at the C-terminus (bottom of figure) have higher order parameters in the apo state than in the $(Cd^{2+})_1$ and $(Ca^{2+})_2$ states. The atom coordinates of the structure were taken from the average solution structure of the $(Ca^{2+})_2$ state (Kördel et al., 1993). The diagram was created with the program MOLSCRIPT (Kraulis, 1991).

MATERIALS AND METHODS

Theory. Relaxation of an amide ^{15}N nucleus spin at high field is dominated by the dipolar interaction with the directly attached proton spin and by the CSA mechanism (Abragam, 1961). The ^{15}N chemical shift tensor is, to a good approximation, axially symmetric with the principal axis nearly collinear with the nitrogen–hydrogen bond (Hiyama et al., 1988). Thus, the relaxation parameters are functions of a spectral density function, $J(\omega)$, that is given by the cosine Fourier transform of the orientational correlation function for a unit vector along the nitrogen–hydrogen bond (Abragam, 1961). The relaxation rate constants, R_1 (spin–lattice or longitudinal relaxation) and R_2 (spin–spin or transverse relaxation), and the steady-state $\{^1H\}$–^{15}N NOE are given by (Abragam, 1961)

$$R_1 = (d^2/4)[J(\omega_H - \omega_N) + 3J(\omega_N) + 6J(\omega_H + \omega_N)] + c^2J(\omega_N) \quad (1)$$

$$R_2 = (d^2/8)[4J(0) + J(\omega_H - \omega_N) + 3J(\omega_N) + 6J(\omega_H) + 6J(\omega_H + \omega_N)] + (c^2/6)[4J(0) + 3J(\omega_N)] + R_{ex} \quad (2)$$

$$\text{NOE} = 1 + (d^2/4R_1)(\gamma_N/\gamma_H)[6J(\omega_H + \omega_N) - J(\omega_H - \omega_N)] \quad (3)$$

[2] The definition of binding equilibria and cooperativity in the calbindin D_{9k} system is given in Figure 5 and elsewhere (Akke et al., 1991; Carlström & Chazin, 1993; Linse et al., 1987, 1991). The macroscopic binding constants K_1 and K_2 can be used to obtain a *lower limit* for the cooperativity as $-\Delta\Delta G = RT \ln (4K_2/K_1)$; as long as K_2 is significantly larger than $0.25K_1$, positive cooperativity prevails (Linse et al., 1987, 1991). Using the values for K_1 and K_2 reported by Kördel et al. (1990), both the P43G mutant and wild-type proteins are seen to bind calcium ions with positive cooperativity, with values of 7.7 ± 1.1 and 5.7 ± 0.7 kJ/mol, respectively.

in which

$$d = \frac{\mu_0 h \gamma_N \gamma_H}{8\pi^2}\left\langle \frac{1}{r_{NH}^3} \right\rangle$$

$$c = \frac{\omega_N}{\sqrt{3}}(\sigma_\parallel - \sigma_\perp)$$

μ_0 is the permeability of free space, h is Planck's constant, γ_H and γ_N are the gyromagnetic ratios of ^1H and ^{15}N, respectively, r_{NH} = 1.02 Å is the nitrogen–hydrogen bond length, ω_H and ω_N are the Larmor frequencies of ^1H and ^{15}N, respectively, and $\sigma_\parallel$ and $\sigma_\perp$ are the components of the chemical shift anisotropy tensor parallel and perpendicular to the bond axis, respectively. In the present work, a value of 160 ppm for the chemical shift anisotropy ($\sigma_\parallel - \sigma_\perp$) [measured for ^{15}N nuclei in helical polypeptide chains (Hiyama et al., 1988; Shoji et al., 1989, 1990)] was used because calbindin D_{9k} is mainly helical (Szebenyi & Moffat, 1986; Kördel et al., 1989; Skelton et al., 1990; Akke et al., 1991). In eq 2, the term R_{ex} has been included to accommodate other pseudo-first-order processes that contribute to the decay of transverse magnetization, such as conformational exchange (Bloom et al., 1965).

The relaxation parameters, R_1, R_2, and NOE, are measured experimentally using proton-detected 2D versions of the inversion recovery, CPMG, and steady-state NOE experiments (Kay et al., 1989; Kördel et al., 1992). The time dependencies of the longitudinal and transverse magnetizations are given by

$$I(t) = I_\infty - [I_\infty - I_0] \exp(-R_1 t) \quad (4)$$

and

$$I(t) = I_\infty + I_0 \exp(-R_2 t) \quad (5)$$

where I_0 is the intensity corresponding to the magnetization at the beginning of the relaxation period t, I_∞ is the steady-state magnetization under the experimental conditions, and R_1 and R_2 are the spin–lattice and spin–spin relaxation rate constants, respectively. In eq 5, the parameter I_∞ has been included to account for possible base-line offsets (Vold & Vold, 1976). The relaxation rate constants are obtained experimentally by fitting eqs 4 and 5 to resonance intensities measured as a function of t. The steady-state NOE is obtained as

$$\text{NOE} = I_{sat}/I_{unsat} \quad (6)$$

where I_{sat} and I_{unsat} are the steady-state intensities measured with and without the saturation of proton magnetization, respectively.

The available experimental data are generally insufficient to determine the spectral density at the five characteristic frequencies in eqs 1–3.[3] Therefore, the spectral density function must be modeled by a simpler function containing the smallest number of motional parameters that reproduce the experimentally determined relaxation parameters, while providing physically meaningful information about the system. The formalisms of the model-free (Lipari & Szabo, 1982a,b) and two-step (Wennerström et al., 1979; Halle & Wennerström, 1981) models provide such treatments by assuming that overall rotational diffusion and internal motions of the bond vectors, both of which contribute to spin relaxation, are independent and that the time scales for internal motions approach the extreme narrowing regime. The more common approach of these former authors, which has been extended to incorporate parameters for internal motional processes on two separable time scales (Clore et al., 1990b), will be followed explicitly. Thus, the spectral density function is modeled as

$$J(\omega) = \frac{2}{5}\left(\frac{S^2 \tau_m}{1 + (\omega\tau_m)^2} + \frac{(S_f^2 - S^2)\tau}{1 + (\omega\tau)^2} \right) \quad (7)$$

where $1/\tau = 1/\tau_m + 1/\tau_e$, and $S^2 = S_f^2 S_s^2$, τ_m is the overall rotational correlation time of the molecule, S^2 is the square of the generalized order parameter describing the restriction of the internal motions, S_f^2 and S_s^2 are the squares of the order parameters for the internal motions on the fast and slow time scales, respectively, and τ_e is the effective correlation time for motions on the slower of these two time scales. Motions on the faster time scale are assumed to be sufficiently fast such that their characteristic correlation times do not contribute significantly to the relaxation parameters. If internal motional processes on two different time scales cannot be resolved, then eq 7 reduces to the original expression (Lipari & Szabo, 1982a) by setting $S_f^2 = 1$. In the following, S^2, S_f^2, and S_s^2 are referred to simply as order parameters. A simple physical interpretation of S^2 is obtained by modeling the internal motions of the N–H bond vector as restricted diffusion within a cone of semiangle θ_0 (Lipari & Szabo, 1980, 1981). For this model

$$S^2 = [(1/2)\cos\theta_0 (1 + \cos\theta_0)]^2 \quad (8)$$

and θ_0 can be calculated from S^2.

An estimate of τ_m can be extracted from the average R_2/R_1 ratio (Kay et al., 1989; Palmer et al., 1991a). The R_2/R_1 ratio for each residue has also been used to provide criteria for the selection of parameters to be included in the optimization of the spectral density function given by eq 7 (Clore et al., 1990a; Palmer et al., 1991a; Kördel et al., 1992). In this study, the statistical approach to selection of parameters introduced by Stone et al. (1992) was applied, as outlined further below.

NMR Spectroscopy. Uniformly ^{15}N-labeled P43G was expressed in *Escherichia coli* grown on M9 minimal media containing $^{15}NH_4Cl$ as the sole source of nitrogen (Skelton et al., 1992) and purified according to Chazin et al. (1989b). The $(Cd^{2+})_1$ sample was prepared as described by Akke et al. (1991). The samples contained 4 mM protein in 95% H_2O/5% D_2O with the pH adjusted to 6.0 by microliter additions of 1 M HCl. The amount of dissolved oxygen was minimized by purging all solvents and containers with argon before preparing the sample.

All experiments were recorded at 300 K on a 11.74 T Bruker AMX 500 spectrometer. The ^{15}N spin–lattice (R_1) and spin–spin (R_2) relaxation constants and the steady-state $\{^1H\}$–^{15}N NOEs were obtained from ^1H-detected ^1H–^{15}N correlation spectra acquired with the sensitivity enhancement protocol (Palmer et al., 1991b; Kördel et al., 1992). This method yields two separate spectra, each with the same signal-to-noise ratio as a conventional experiment recorded in the same amount of time. The two spectra can be added together to give a final spectrum with a $(2)^{1/2}$ higher signal-to-noise ratio than a conventional experiment or, alternatively, the two spectra can be analyzed separately, allowing two independent measurements in the same amount of time as a single conventional experiment. The former alternative was used for the R_1 and R_2 measurements, whereas the latter approach was taken for the NOE measurements. The pulse sequences are given in Kördel et al. (1992). In short, the R_1 and R_2 experiments consist of a refocused INEPT sequence (Morris & Freeman,

[3] A strategy for direct sampling of the spectral density at distinct frequencies has recently been proposed by Peng and Wagner (1992a,b).

1979; Burum & Ernst, 1980) to transfer magnetization from the amide protons to the ^{15}N nuclei, a variable relaxation period (t), a t_1 evolution period, and a sensitivity-enhanced INEPT sequence to transfer ^{15}N magnetization back to the amide protons for detection [Figure 2a,b of Kördel et al. (1992)]. GARP-1 decoupling (Shaka et al., 1985) of the protons was applied during the relaxation period of the inversion recovery experiments in order to eliminate the effects of dipolar cross-relaxation and cross-correlation between the dipolar and anisotropic chemical shift relaxation mechanisms (Boyd et al., 1990). An ^{15}N CPMG spin–echo sequence (Carr & Purcell, 1954; Meiboom & Gill, 1958) was applied during the transverse relaxation period of the R_2 experiments. The delay between the refocusing pulses was set to 1 ms, which is sufficiently short to effectively eliminate the effects of evolution under the heteronuclear scalar coupling Hamiltonian (Vold & Vold, 1976; Kay et al., 1992; Palmer et al., 1992). The effects of cross-correlation on the ^{15}N transverse relaxation were suppressed by the application of ^1H 180° pulses synchronously with the even echoes in the CPMG sequence (Kay et al., 1992; Palmer et al., 1992). The NOE experiment consists of an initial recovery period, a t_1 evolution period, and a sensitivity-enhanced INEPT to transfer magnetization from the ^{15}N nuclei to the amide protons for detection [Figure 2c of Kördel et al. (1992)]. Spectra were acquired with and without irradiation of the protons using GARP-1 during the recovery period to measure I_{sat} and I_{unsat}, respectively. These spectra were acquired in an interleaved fashion to minimize differences in sample conditions.

All spectra were recorded with a spectral width of 12 500 Hz over 2048 complex points in ω_2 and the carrier set on the H_2O signal. Digital oversampling by a factor of 2 was used to reduce base-line distortions associated with the spectrometer's low-pass filters (Delsuc & Lallemand, 1986). Water suppression was achieved by applying 0.5–1.0-ms spin-lock purge pulses (Otting & Wüthrich, 1988; Messerle et al., 1989). The spectral width in ω_1 was 1250 Hz, sampled over a total of 300 t_1 points using the TPPI method for frequency discrimination (Marion & Wüthrich, 1983). The delay for the INEPT polarization transfers was set to 2.7 ms, and the ^{15}N nuclei were decoupled during the acquisition period using the WALTZ-16 sequence (Shaka et al., 1983). For the R_1 and R_2 experiments, the sum of the recycle delay and acquisition time was set to 3.3 s (approximately 3 times the longest ^1H spin–lattice relaxation time), and the total number of FIDs recorded per t_1 point was 8. For the NOE experiment, the ^1H recovery period prior to acquisition was 4.6 s (greater than 8 times the longest ^{15}N spin–lattice relaxation time), and the total number of FIDs recorded per t_1 point was 32.

For the apo state, nine R_1 experiments using seven different relaxation delays were performed [0.03 (×3), 0.11, 0.24, 0.48, 0.96, 1.50, and 2.94 s]. The R_2 values for the apo state were obtained from eight experiments using seven relaxation delays [0.004 (×2), 0.032, 0.092, 0.180, 0.300, 0.702, and 1.300 s]. For the $(Cd^{2+})_1$ state, the R_1 values were determined from a set of twelve experiments using eight different relaxation delays [0.03 (×2), 0.11, 0.39, 0.73 (×2), 1.12, 2.01 (×2), and 3.02 s (×2)], and the R_2 values were determined from a set of ten experiments using eight relaxation delays [0.004 (×2), 0.032, 0.074, 0.128, 0.220, 0.356, 0.800, and 1.300 (×2) s]. The duplicate experiments were used to evaluate the uncertainty in the peak heights (Palmer et al., 1991a; Skelton et al., 1993, *vide infra*). The third R_1 experiment with t = 0.03 s for the apo state was recorded 4 days after the other two, in order to assess whether the measurements of the relaxation data were affected by the lower long-term stability of the apoprotein. Four independent determinations of the NOE were made from two sensitivity-enhanced experiments for both the apo and $(Cd^{2+})_1$ states.

Data Processing and Analysis. The data were processed with in-house modified versions of the FTNMR software (Hare Research, Inc.) running on Convex C240 and Sun SPARCstation SLC computers. The data were zero-filled prior to Fourier transform in both dimensions to yield a final matrix of 4096 × 2048 real data points. The first point in each row and column was halved before Fourier transform to suppress ridges (Otting et al., 1986), and a low-pass filter was used to suppress the solvent signal in the time domain data (Marion et al., 1989). To optimize sensitivity for resolved resonances, a matched 6 Hz exponential filter was applied in ω_2 and a cosine bell window function was applied in ω_1. To optimize resolution for overlapped resonances while keeping the uncertainty of the peak intensities at an acceptable level [see the guidelines given by Skelton et al. (1993)], a Lorentzian–Gaussian window function was applied in ω_2, and the ω_1 interferograms were extended to 600 points using the HSVD linear prediction algorithm (Barkhuijsen et al., 1987) prior to application of the cosine bell filter.

Relaxation rate constants and NOEs were obtained from the cross-peak intensities measured as peak heights in the ^1H–^{15}N correlation spectra. The uncertainties in the measured peak heights were estimated from the duplicate spectra. The uncertainty in the peak height, σ_h, is given by $1/(2)^{1/2}$ times the standard deviation of the differences between corresponding cross-peak heights in pairs of spectra acquired under identical conditions (Palmer et al., 1991a). As noted previously (Stone et al., 1992; Kördel et al., 1992; Skelton et al., 1993), σ_h generally decreased with the length of the relaxation period. For the apo state, the value of σ_h determined for t = 0.03 s was used for all relaxation delays. For the $(Cd^{2+})_1$ state, σ_h was determined for four of the relaxation delays and was estimated by interpolation for the others. Nonlinear optimization of eqs 4 and 5 to fit the experimental data was carried out with the Levenberg–Marquardt algorithm (Press et al., 1986). The methods described in Palmer et al. (1991a) were used to estimate the uncertainties in the relaxation rates and to evaluate the statistical fits between the monoexponential functions and the experimental data. The mean values and standard deviations of the NOEs were calculated from four independent measurements using eq 6.

Analysis of the relaxation data within the model-free formalism was performed by minimizing the sum-squared-error (SSE) between the experimental data and relaxation parameters calculated using eqs 1–3 and 7, as described by Palmer et al. (1991a). The SSE was calculated as the sum of the squares of the weighted differences between the experimental and predicted relaxation parameters, in which the weights were obtained from the experimental uncertainties in the relaxation measurements. The uncertainties of the optimized model-free parameters were estimated by Monte Carlo simulations of 500 samples (Palmer et al., 1991a). The model-free analysis was carried out in three stages (Stone et al., 1992); (i) initially, S^2 and τ_e were optimized with S_f^2 fixed at unity for all residues and τ_m fixed at the value obtained from the R_2/R_1 ratio; (ii) as in (i), but with τ_e included only for residues that had a value of τ_e in stage (i) of more than 2 standard deviations greater than zero and with an exchange term, R_{ex}, included for all residues; (iii) as in (ii), but with R_{ex} included only for residues that had a value of R_{ex} in stage (ii) of more than 2 standard deviations greater than the uncertainty of the experimental value for R_2 and with S_f^2 allowed to deviate from unity for those residues that had an

R_2/R_1 ratio more than 1 standard deviation below the average or an SSE in stage (ii) more than 1 standard deviation above the average. The final evaluation of the model-free analysis was performed by simultaneously optimizing the overall rotational correlation time and the internal motional parameters selected for each individual residue. ^{15}N relaxation data for $(Ca^{2+})_2$-calbindin D_{9k} have been acquired at both 11.74 and 14.10 T (Kördel et al., 1992). In order to make an unbiased intercomparison of the three states of the protein, only the data acquired at 11.74 T were used for the model-free analysis presented here.

Statistical Analysis. The model-free results for the four helices and the two ion-binding loops were analyzed statistically to assess the dependence of S^2 and τ_e on the structural elements and/or number of bound ions. The structural elements included in this analysis were helix I (E4–A14), ion-binding loop I (K16–S24), helix II (K25–E35), helix III (L46–D54), ion-binding loop II (K55–S62), and helix IV (F63–I73); the flexible linker loop (F36–T45) and residues near the N- and C-termini (M0, K1, S2, S74, and Q75) were excluded from this analysis. In essence, the statistical analysis determines whether the model-free parameters (regarded as functions of structural elements and/or number of bound ions) are adequately described by the grand mean values for the order parameters and effective correlation times calculated over the 18 combinations of structural elements and ion levels (four helices and two ion-binding loops for each of the three ion levels). If the model-free parameters are not described adequately by the grand mean values, the analysis further addresses whether the data are described adequately by the mean values for the three ion levels (calculated over all structural elements) or by the mean values for the six structural elements (calculated over all ion levels). If the data are not described adequately by the mean values for the three ion levels or the six structural elements, the conclusion is reached that the data are adequately described only by the set of 18 means for the order parameters and 18 means for the effective correlation times in each combination of structural element and ion loading.

To account for correlations between the model-free parameters for corresponding residues in the apo, $(Cd^{2+})_1$, and $(Ca^{2+})_2$ states, repeated-measure ANOVA analyses (Cole & Grizzle, 1966; Winer, 1991), rather than conventional ANOVA procedures, were performed. The following null hypotheses were tested: (1) model-free parameters are independent of structural elements; (2) model-free parameters are independent of ion loading; and (3) the interacting effects of structural elements and ion loading on model-free parameters are negligible. When any of the above three null hypotheses were rejected, then additional statistical tests were used to identify particular subsets of the individual means that differ significantly from each other. Model-free results for each state of calbindin D_{9k} were compared using Helmert contrasts, in which the results for the apo state were compared to the mean results for the metal-bound states and the results for the $(Cd^{2+})_1$ state were compared to the results for the $(Ca^{2+})_2$ state. Model-free parameters for individual structural elements within a single ion state were compared using pairwise comparisons and Tukey's method for controlling type I errors (Devore, 1982). Model-free parameters for individual structural elements were compared between the different ion-binding states using Helmert contrasts with paired *t*-tests; Bonferroni's method was used to control type I errors (Devore, 1982). All analyses were performed by using the SAS statistical package (SAS Institute, Cary, NC).

RESULTS

Complete ^{15}N resonance assignments for apo- and $(Cd^{2+})_1$-calbindin D_{9k} have been reported previously (Skelton et al., 1992b); hence, ^{15}N relaxation data could be analyzed for nearly every residue. In both the apo and $(Cd^{2+})_1$ states [as well as the $(Ca^{2+})_2$ state], residue K01 is broadened beyond detection by solvent exchange. In the $(Cd^{2+})_1$ state, cross-peaks are also not detected for E17 and S24 (in loop 1) due to severe exchange broadening in the ^1H dimension; thus, relaxation parameters could not be obtained for these residues. Furthermore, in the $(Cd^{2+})_1$ state, a number of cross-peaks from residues in loop I show exchange broadening in the ^{15}N dimension: A15 and L23 are significantly broadened, while A14, K16, G18, D19, and Q22 are slightly broadened. A further discussion of these effects is given below.

Severe spectral overlap of cross-peaks in the ^1H–^{15}N correlation spectra is observed for L23/L32 and L28/S62 in the apo state and I09/L39 and L32/F66 in the $(Cd^{2+})_1$ state. All overlaps except the I09/L39 pair in the $(Cd^{2+})_1$ state could be resolved by the resolution enhancement procedure described above (Skelton et al., 1993), and reliable relaxation parameters could be measured for each nucleus. Only one set of relaxation data and model-free parameters is reported for I09 and L39, as derived from the summed cross-peak. A smaller degree of overlap is observed for K12/L40, K29/E60, and N56/Q67 in the apo state and A14/L49, S38/T45, S44/D47, and E51/Q67 in the $(Cd^{2+})_1$ state. Although these latter pairs of partially overlapped cross-peaks appeared to be moderately well resolved from each other in the spectra processed to maximize sensitivity, monoexponential relaxation functions were not sufficient to describe the experimental data. After reprocessing using the resolution-enhancement protocol, the data were well described by monoexponential functions.

One additional experiment was necessary to verify that the lower long-term stability of the apoprotein, as compared with the $(Ca^{2+})_2$ and $(Cd^{2+})_1$ states, did not have an adverse effect on the experimental data. The triplicate acquisition of the inversion recovery experiment with the shortest relaxation delay showed that the uncertainty of the measured peak heights increased by only ~3% over 4 days; thus, the apoprotein is sufficiently stable as to not introduce any significant errors in the subsequent analysis.

The R_1 and R_2 relaxation rate constants and NOEs for apo- and $(Cd^{2+})_1$-calbindin D_{9k} are reported in Table S1 of the supplementary material. In the following, the relaxation parameters obtained at 11.74 T for the $(Ca^{2+})_2$ state are also included to facilitate comparisons. Figure 2 shows representative relaxation curves for residue G57 in the three ion-binding states of the protein. The ranges of R_1 values measured are 1.72–2.68 (apo), 1.41–2.71 [$(Cd^{2+})_1$], and 1.47–2.61 s^{-1} [$(Ca^{2+})_2$]. Excluding the residues for which the double internal time scale has been invoked (*vide infra*), the average values and the standard deviations of R_1 are 2.49 ± 0.11, 2.53 ± 0.15, and 2.50 ± 0.09 s^{-1}, respectively. The ranges of R_2 values for the residues without appreciable exchange contributions are 2.90–6.62 (apo), 2.05–6.50 [$(Cd^{2+})_1$], and 2.01–6.25 s^{-1} [$(Ca^{2+})_2$ state)]. Excluding residues for which the double internal time scale has been invoked and residues with significant exchange contributions to relaxation, the average values and standard deviations of R_2 are 5.45 ± 0.78, 5.73 ± 0.58, and 5.80 ± 0.30 s^{-1}, respectively. In the $(Cd^{2+})_1$ state, Q75 is the only residue that exhibits a negative NOE, as is also the case in the $(Ca^{2+})_2$ state. No residues with negative NOEs are found in the apo state, but Q75 does have the lowest NOE value (0.109). The ranges of NOEs for the other residues are 0.248–0.824 (apo), 0.253–0.780 [$(Cd^{2+})_1$], and 0.246–

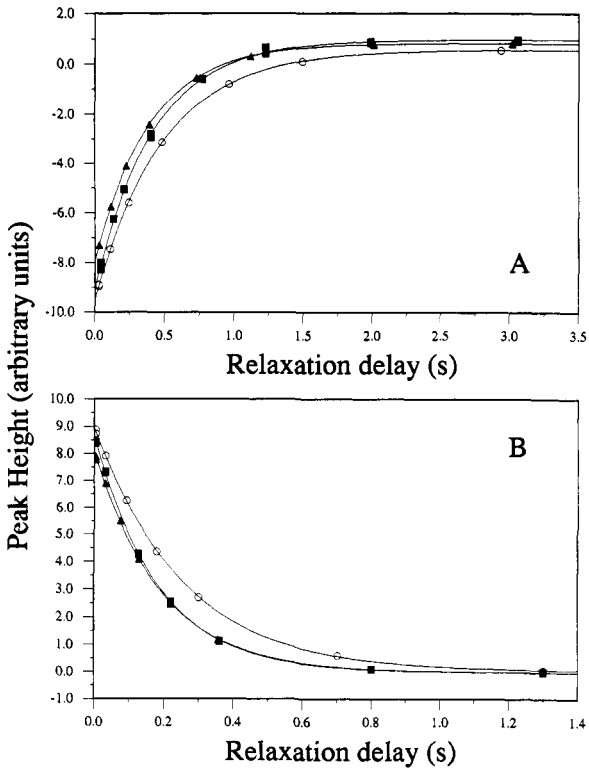

FIGURE 2: Typical relaxation decay curves for residue G57 in apo (○), $(Cd^{2+})_1$ (▲), and $(Ca^{2+})_2$ (■) calbindin D_{9k}. Panel A shows the results for the inversion recovery R_1 measurements. Panel B shows the results of the CPMG R_2 measurements. The curves represent optimized monoexponential functions. Peak heights are given in arbitrary units with an uncertainty smaller than the size of the symbols. The duplicate data pairs taken for some relaxation delays (see the text) are included in the figures.

0.758 [$(Ca^{2+})_2$]. Excluding residues fit with extended model-free parameters, the averages and standard deviations are 0.678 ± 0.051, 0.689 ± 0.068, and 0.700 ± 0.050, respectively. The preliminary values of τ_m determined from the R_2/R_1 ratio were 4.20 ns for the apo state and 4.17 ns for the $(Cd^{2+})_1$ state, as compared to 4.15 ns for the $(Ca^{2+})_2$ state.

The model-free parameters (S^2 and τ_e) and exchange terms (R_{ex}) for the apo and $(Cd^{2+})_1$ states are listed in Table I. The optimized global values of τ_m were 4.10 ± 0.01 ns for the apo state and 4.10 ns for the $(Cd^{2+})_1$ state. The Monte Carlo simulations did not provide a reliable estimate of the uncertainty in τ_m for the $(Cd^{2+})_1$ state; however, the uncertainty is expected to be comparable to that determined for the other two states. The values for τ_m are in good agreement with the value of 4.25 ± 0.04 ns for the $(Ca^{2+})_2$ state (Kördel et al., 1992), as well as with the values obtained from the R_2/R_1 ratios. The extended model-free parameters S_f^2, S_s^2, and τ_e are given in Table II for residues K41, G42, G43, S44, G57, D58, G59, and Q75 for the apo state and K41, G42, G43, and Q75 for the $(Cd^{2+})_1$ state. Since the value of R_2 could not be determined with satisfactory confidence for A15 and L23 in the $(Cd^{2+})_1$ state due to an exchange contribution, these residues were not included in the model-free analysis. In both the apo and $(Cd^{2+})_1$ states, Q75 appears to exhibit internal motions on two separable time scales in the 10^{-12}–10^{-9} s range, as well as conformational exchange indicative of internal motions on a time scale of 10^{-6}–10^{-3} s. In order to achieve a reasonably good fit, as determined by the residual SSE, the experimental R_2 was excluded and the model-free parameters S_s^2 and τ_e were optimized while S_f^2 and τ_m were kept fixed. The analysis was performed using values of S_f^2 ranging from 0.30 to 0.95 in steps of 0.05. The results from this analysis showed that, for all values of S_f^2 that yield a low SSE, S^2 (the product of S_f^2 and S_s^2) was constant to within ± 0.08. Thus, while the value of S^2 is well determined, the precision of the values of S_f^2, S_s^2, and τ_e for Q75 is unknown.

The goodness-of-fit between the model-free analysis and the experimental relaxation data was evaluated by comparing the experimentally determined relaxation parameters and those predicted from the model-free parameters. The mean SSE per residue was 3.7 and 5.8 for the apo and $(Cd^{2+})_1$ states, respectively, corresponding to average deviations between the experimental and predicted relaxation parameters of less than 1.1 and 1.4 times the experimental uncertainties in the relaxation parameters. The RMS differences between the experimental and predicted values for each relaxation parameter are, for the apo and $(Cd^{2+})_1$ states, respectively: 0.07 (3%) and 0.01 s^{-1} (0.4%) for R_1; 0.11 (2%) and 0.25 s^{-1} (4%) for R_2; 0.016 (3%) and 0.011 (2%) for NOE. Thus, the model-free formalism applied in this study is sufficient to describe the relaxation data accurately.

The analysis of the backbone dynamics of $(Ca^{2+})_2$-calbindin D_{9k} from ^{15}N relaxation data was based on data obtained at 11.74 and 14.10 T (Kördel et al., 1992). In order to perform an unbiased comparison of the three states of the protein, the model-free parameters for the $(Ca^{2+})_2$ state were reoptimized using only data obtained at 11.74 T, following the criteria for selection of model-free parameters outlined above for the apo and $(Cd^{2+})_1$ states. This resulted in the inclusion of an R_{ex} term for 42 residues, which is a larger number than those for the apo (14) and $(Cd^{2+})_1$ (21) states. However, all of these contributions are very small (in no case is the value of R_{ex} greater than 0.33 s^{-1}), and inclusion of the R_{ex} terms for the $(Ca^{2+})_2$ state does not affect significantly the model-free parameters (*vide infra*). Extended model-free parameters were invoked for residues G42, G43, S74, and Q75, with Q75 treated as for the apo and $(Cd^{2+})_1$ states. The order parameters and internal correlation times for these four residues are listed in Table II.

As a control, a separate optimization of the model-free parameters for the $(Ca^{2+})_2$ state was performed using the relaxation data obtained at 11.74 T, but with the selection of model-free parameters based on the criteria used by Kördel et al. (1992), in which no R_{ex} terms were included. The resulting values of S^2 and τ_e did not differ significantly from those obtained from the optimization of the parameters chosen according to the criteria used for the apo and $(Cd^{2+})_1$ states; the average difference between order parameters obtained from the two optimizations is 0.002, with a standard deviation of ± 0.014. [Since τ_e refers to different time scales in the extended and original model-free formalisms, this statement does not apply to those residues for which the extended model was invoked in one of the treatments but not the other.] The model-free parameters obtained from data acquired at two magnetic fields and those obtained from data acquired at one magnetic field differ significantly only for residues G42, G43, S44, and Q75. For each of these residues, the values of S^2 are lower and the values of τ_e are higher when relaxation data from two fields are included in the optimization. In all three optimizations performed, the optimized global value of τ_m was 4.25 ± 0.01 ns.

A plot comparing the generalized order parameters for apo-, $(Cd^{2+})_1$-, and $(Ca^{2+})_2$-calbindin D_{9k} is shown in Figure 3, and the values of τ_e for the three states are plotted in Figure 4. Substantial differences in the order parameters measured for the three states are observed for residues G57, D58, G59, and E60 in loop II and for S74 and Q75 at the C-terminus. In both regions the apo state differs from the other two states,

Table I: Model-Free Parameters for Apo and $(Cd^{2+})_1$ P43G Calbindin D_{9k} and Categorization According to Amide Proton Exchange Rates[a]

	apo				$(Cd^{2+})_1$			
residue	S^2	τ_e (ps)	R_{ex} (s^{-1})[b]	HX[c]	S^2	τ_e (ps)	R_{ex} (s^{-1})[b]	HX[c]
S02	0.71 ± 0.03	48.4 ± 2.2		○	0.71 ± 0.03	58.5 ± 2.5		○
E04	0.78 ± 0.04	34.8 ± 1.6		⊗	0.79 ± 0.04	44.3 ± 2.1		⊗
E05	0.79 ± 0.04	41.1 ± 2.1		⊗	0.80 ± 0.04	51.4 ± 2.3		⊗
L06	0.82 ± 0.04	44.6 ± 1.9		⊗	0.83 ± 0.04	47.5 ± 2.0		⊗
K07	0.87 ± 0.04	0.0 ± 0.6		⊗	0.85 ± 0.04	10.6 ± 0.5		⊗
G08	0.87 ± 0.04	4.9 ± 0.0	0.48 ± 0.02	⊗	0.88 ± 0.04		0.75 ± 0.04	⊗
I09	0.84 ± 0.04	25.4 ± 1.2		×	0.87 ± 0.04	19.2 ± 0.9		×
F10	0.87 ± 0.04	14.3 ± 1.7		×	0.88 ± 0.04	16.0 ± 0.6		×
E11	0.90 ± 0.04	0.0 ± 0.0		×	0.90 ± 0.04	19.2 ± 1.0		×
K12	0.85 ± 0.04	23.8 ± 0.8		×	0.86 ± 0.04	24.1 ± 1.1	0.39 ± 0.02	×
Y13	0.86 ± 0.04	20.0 ± 0.7		×	0.86 ± 0.04	17.4 ± 1.0		×
A14	0.87 ± 0.04	35.9 ± 1.8	0.44 ± 0.02	×	0.88 ± 0.04		3.34 ± 0.15	×
A15	0.83 ± 0.04	33.0 ± 1.5	2.39 ± 0.10	×	nd	nd	ex	nd
K16	0.82 ± 0.04	31.9 ± 1.2	0.40 ± 0.02	⊗	0.78 ± 0.03	26.4 ± 0.5	7.61 ± 0.40	⊗
E17	0.78 ± 0.04	35.9 ± 1.8	0.89 ± 0.03	⊗	nd	nd	nd	nd
G18	0.78 ± 0.04	18.6 ± 0.0		⊗	0.81 ± 0.04		12.55 ± 0.49	⊗
D19	0.73 ± 0.03	26.6 ± 1.4	1.32 ± 0.05	○	0.81 ± 0.03		10.90 ± 0.60	⊗
N21	0.82 ± 0.04	14.4 ± 1.1		⊗	0.83 ± 0.04	12.5 ± 0.7	0.73 ± 0.03	⊗
Q22	0.83 ± 0.04	40.0 ± 2.4		⊗	0.84 ± 0.04	13.4 ± 0.6	4.52 ± 0.21	×
L23	0.85 ± 0.04	13.4 ± 2.0		×	nd	nd	ex	nd
S24	0.85 ± 0.04	0.0 ± 1.5		⊗	nd	nd	nd	nd
K25	0.86 ± 0.04	33.4 ± 1.5		⊗	0.87 ± 0.04	3.7 ± 0.3		⊗
E26	0.84 ± 0.04	19.2 ± 0.7		⊗	0.85 ± 0.04			⊗
E27	0.88 ± 0.04			×	0.88 ± 0.04		0.50 ± 0.01	×
L28	0.89 ± 0.04			×	0.89 ± 0.04	7.8 ± 0.1	0.92 ± 0.04	×
K29	0.88 ± 0.04	6.3 ± 0.4		×	0.90 ± 0.04	6.4 ± 0.9	0.57 ± 0.03	×
L30	0.85 ± 0.04		0.33 ± 0.01	×	0.88 ± 0.04			×
L31	0.89 ± 0.04	16.7 ± 0.8		×	0.90 ± 0.04	13.4 ± 0.6		×
L32	0.92 ± 0.04			×	0.89 ± 0.04	15.2 ± 0.3		×
Q33	0.86 ± 0.04	15.1 ± 1.0		×	0.87 ± 0.04	25.7 ± 1.2		×
T34	0.84 ± 0.04	8.8 ± 0.0		×	0.87 ± 0.04		0.44 ± 0.00	×
E35	0.82 ± 0.04	20.1 ± 1.2	0.56 ± 0.03	×	0.88 ± 0.04			×
F36	0.84 ± 0.04	4.3 ± 0.0		×	0.82 ± 0.04	10.0 ± 0.4		×
S38	0.83 ± 0.04	37.1 ± 1.5		⊗	0.85 ± 0.04	0.3 ± 0.4		⊗
L39	0.81 ± 0.04	47.5 ± 2.6		⊗	0.87 ± 0.04	19.2 ± 0.6		⊗
L40	0.73 ± 0.03	76.4 ± 3.2		○	0.76 ± 0.03	72.2 ± 3.2		⊗
K41	0.60 ± 0.07	*		○	0.68 ± 0.07	*		○
G42	0.50 ± 0.07	*		○	0.53 ± 0.07	*		○
G43	0.49 ± 0.06	*		○	0.56 ± 0.07	*		○
S44	0.61 ± 0.07	*		○	0.58 ± 0.03	55.5 ± 2.4		○
T45	0.74 ± 0.03	61.0 ± 2.8		○	0.73 ± 0.03	43.7 ± 1.9		○
L46	0.80 ± 0.04	50.5 ± 2.2		⊗	0.86 ± 0.04	12.0 ± 0.3		⊗
D47	0.80 ± 0.04	23.7 ± 1.3		⊗	0.84 ± 0.04	10.2 ± 0.4		⊗
E48	0.81 ± 0.04	35.6 ± 1.4		⊗	0.85 ± 0.04	21.9 ± 1.0		⊗
L49	0.82 ± 0.04	43.7 ● 2.3		×	0.87 ± 0.04	22.3 ± 1.0		×
F50	0.83 ± 0.04	55.4 ± 2.8		×	0.88 ± 0.04	16.8 ± 0.7		×
E51	0.84 ± 0.04	22.8 ± 0.3	0.56 ± 0.02	⊗	0.87 ± 0.04	43.5 ± 1.3	0.31 ± 0.02	×
E52	0.83 ± 0.04	58.3 ± 2.6		⊗	0.86 ± 0.04	11.0 ± 0.4		×
L53	0.82 ± 0.04	44.8 ± 2.1		⊗	0.86 ± 0.04	29.1 ± 1.5	0.41 ± 0.02	×
D54	0.80 ± 0.04	30.0 ± 0.0	0.33 ± 0.01	⊗	0.88 ± 0.04	0.0 ± 0.0		×
K55	0.74 ± 0.03	47.2 ± 1.8	1.11 ± 0.05	○	0.81 ± 0.04	1.1 ± 0.0	1.17 ± 0.05	×
N56	0.80 ± 0.04	22.0 ± 2.0		⊗	0.85 ± 0.04	10.1 ± 0.0	0.88 ± 0.04	×
G57	0.59 ± 0.07	*		○	0.84 ± 0.04			×
D58	0.63 ± 0.07	*		○	0.86 ± 0.04			⊗
G59	0.62 ± 0.07	*		○	0.90 ± 0.04			×
E60	0.69 ± 0.03	41.6 ± 2.0		○	0.88 ± 0.04			×
V61	0.81 ± 0.04	30.8 ± 1.5	1.11 ± 0.05	×	0.87 ± 0.04			×
S62	0.90 ± 0.04	4.9 ± 0.5		×	0.90 ± 0.04		1.16 ± 0.05	×
F63	0.88 ± 0.04			⊗	0.88 ± 0.04			⊗
E64	0.85 ± 0.04	5.7 ± 1.0		⊗	0.86 ± 0.04	6.0 ± 0.4		⊗
E65	0.87 ± 0.04	7.0 ± 0.3		×	0.85 ± 0.04		3.13 ± 0.16	×
F66	0.89 ± 0.04	0.4 ± 0.2		×	0.91 ± 0.04			×
Q67	0.90 ± 0.04			×	0.88 ± 0.04	0.0 ± 0.2		×
V68	0.85 ± 0.04		0.32 ± 0.02	×	0.88 ± 0.04	25.2 ± 1.1	0.40 ± 0.02	×
L69	0.89 ± 0.04	31.3 ± 1.3		×	0.87 ± 0.04	38.1 ± 2.0		×
V70	0.87 ± 0.04	28.1 ± 2.8		×	0.84 ± 0.04	46.6 ± 1.9	1.99 ± 0.08	×
K71	0.90 ± 0.04	41.1 ± 1.8		×	0.83 ± 0.04	42.9 ± 1.7	0.50 ± 0.02	⊗
K72	0.82 ± 0.04	43.7 ± 1.8		×	0.77 ± 0.04	70.0 ± 3.2		⊗
I73	0.79 ± 0.04	39.7 ± 1.9	0.65 ± 0.02	⊗	0.73 ± 0.03	79.1 ± 3.5		○
S74	0.77 ± 0.04	65.0 ± 2.6		⊗	0.67 ± 0.03	83.1 ± 3.6		○
Q75	0.44 ± 0.03	*		○	0.33 ± 0.02	*		○

[a] The generalized order parameter, $S^2 = S_f^2 S_s^2$. For all residues except those with an asterisk in the τ_e column, $S_f^2 = 1$ and $S^2 = S_s^2$. For residues with an asterisk in the τ_e column, S_f^2 was included as a model-free parameter, and the effective correlation time for the internal motions on the faster of the two time scales was assumed to be sufficiently fast (<10 ps) to contribute insignificantly to the relaxation parameters. For these residues, S_f^2, S_s^2, and τ_e are given in Table II. The notation "nd" indicates values not determined due to chemical exchange (see the text). [b] ex indicates that the conformational exchange is too fast to allow optimization of model-free parameters. [c] Rates of amide proton exchange with solvent and order parameters are categorized using the following symbols: ○, $k_{ex} > 0.01$ s^{-1} and $S^2 < 0.75$; ⊗, $k_{ex} > 0.01$ s^{-1} and $S^2 > 0.75$; ×, $k_{ex} < 0.01$ s^{-1} and $S^2 > 0.75$.

Table II: Extended Model-Free Parameters for Apo-, $(Cd^{2+})_1$-, and $(Ca^{2+})_2$-calbindin D_{9k}

residue	S_f^2	S_s^2	τ_e (ps)
	Apo		
K41	0.80 ± 0.04	0.75 ± 0.03	152 ± 8
G42	0.97 ± 0.04	0.51 ± 0.02	74 ± 3
G43	0.89 ± 0.04	0.55 ± 0.02	85 ± 4
S44	0.73 ± 0.03	0.84 ± 0.04	283 ± 13
G57	0.77 ± 0.03	0.77 ± 0.03	150 ± 7
D58	0.78 ± 0.03	0.81 ± 0.04	144 ± 8
G59	0.83 ± 0.04	0.74 ± 0.03	157 ± 8
Q75	0.70[a]	0.63 ± 0.03	592 ± 27
	$(Cd^{2+})_1$		
K41	0.84 ± 0.04	0.81 ± 0.04	157 ± 7
G42	0.93 ± 0.04	0.57 ± 0.03	95 ± 4
G43	0.80 ± 0.03	0.70 ± 0.03	138 ± 7
Q75	0.70[a]	0.47 ± 0.02	305 ± 14
	$(Ca^{2+})_2$		
G42	0.80 ± 0.04	0.55 ● 0.03	88 ± 4
G43	0.70 ● 0.03	0.66 ± 0.03	116 ± 5
S74	0.77 ± 0.03	0.78 ● 0.03	150 ± 7
Q75	0.70[a]	0.48 ± 0.02	392 ± 19

[a] S_f^2 was kept fixed at this value for Q75 during the optimization of the model-free parameters; see the text for details.

with lower values of S^2 in loop II but higher values at the C-terminus.

The average values of the order parameters and internal correlation times for the four helices and the two ion-binding loops of calbindin D_{9k} are presented in Table III, to allow comparisons between the structural elements for a given level of ion loading and intercomparisons for a particular structural element between the three ion-binding states. For loop II in the apo state, the average order parameter is significantly smaller and the average internal correlation time is substantially longer than the corresponding values for the other structural elements. The average order parameters for the other structural elements vary by only small amounts for different levels of ion occupancy. Helix II exhibits a consistently higher average order parameter than the other structural elements; otherwise, pairwise comparisons do not reveal any specific trends in the average model-free parameters.

The statistical significance of the differences in the mean values of the model-free parameters was assessed further using a repeated-measures analysis of variance (Table IV). The results of this analysis show that the mean values of the order parameters and internal correlation times are dependent on both the structural elements of the protein and the number of ions bound. Thus, the data are adequately described only by the set of 18 means of order parameters and 18 means of effective correlation times in each combination of structural element and ion loading. The most important insights obtained from the paired *t*-tests of the Helmert contrasts for individual structural elements (Table V) are that the average order parameter is significantly lower and the average internal correlation time is significantly longer for helix III in the apo state than in the metal-bound states. In addition, the average order parameters for helix II, helix III, and helix IV are larger in the $(Cd^{2+})_1$ state than in the $(Ca^{2+})_2$ state. Although the differences in mean order parameters for these helices are small (0.02–0.03), the results are statistically significant, since Bonferroni's method has been used to control the overall type I error for multiple comparisons.

DISCUSSION

Results from the ^{15}N spin relaxation measurements on apo-, $(Cd^{2+})_1$-, and $(Ca^{2+})_2$-calbindin D_{9k} enable the assessment of response of the intramolecular dynamics of the backbone N–H bond vectors of the protein to the binding of ions. These results are summarized by the shading on the ribbon diagram of the three-dimensional structure of the protein in Figure 1. In the following discussion, emphasis will be placed on intercomparisons between the three ion-binding states of the protein in order to address possible contributions to the cooperativity in Ca^{2+} binding by calbindin D_{9k}. A more general discussion that relates ^{15}N spin relaxation results for calbindin D_{9k} to relaxation studies from other laboratories, RMS deviations in the NMR-derived solution structure of calbindin D_{9k}, and *B* factors in the calbindin D_{9k} X-ray crystal structure has been presented elsewhere for the $(Ca^{2+})_2$ state (Kördel et al., 1992).

Effects of Ion Level on Model-Free Parameters. The most dramatic effect of ion binding on the high-frequency (10^9–10^{12} s^{-1}) internal dynamics of calbindin D_{9k} is the large increase in order parameters observed for loop II in the $(Cd^{2+})_1$ state compared with that in the apo state. For residues G57–E60,

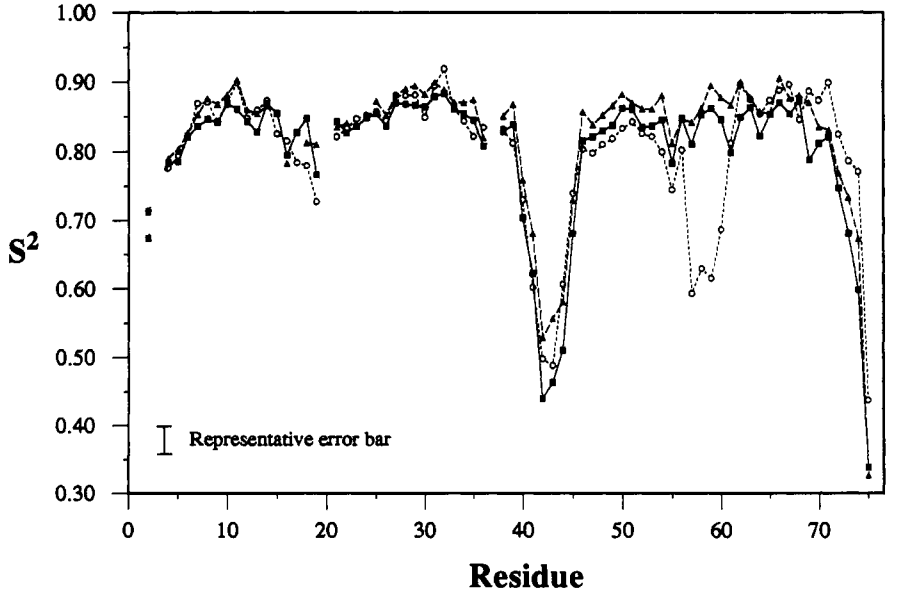

FIGURE 3: Comparison of the generalized order parameters (S^2) for apo (○), $(Cd^{2+})_1$ (▲), and $(Ca^{2+})_2$ (■) calbindin D_{9k}. A representative error bar is shown on the bottom left-hand side of the figure. Residues optimized with the extended model-free model have uncertainties 1.5 times the size of the error bar shown. Breaks in the lines occur at the three prolines, P3, P20, and P37, in all three states and at A15, E17, and L23–S24 in the $(Cd^{2+})_1$ state (see the text).

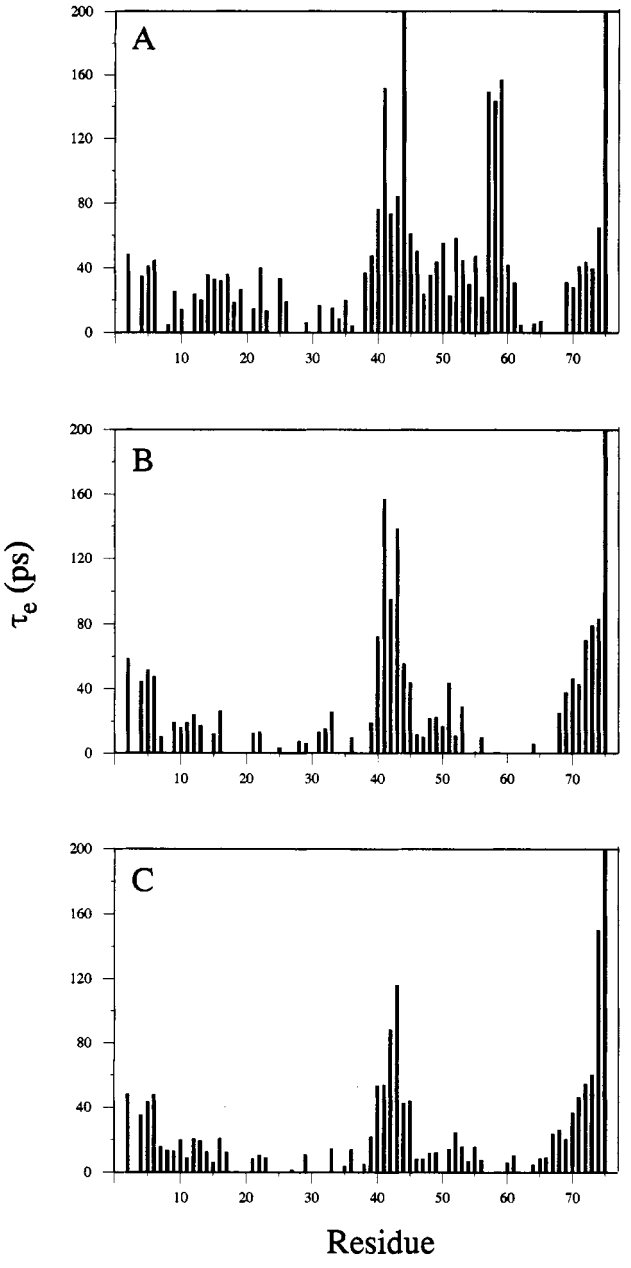

FIGURE 4: Comparison of the effective internal correlation times (τ_e) for (A) apo, (B) $(Cd^{2+})_1$, and (C) $(Ca^{2+})_2$-calbindin D_{9k}. For clarity, the largest data bar has been truncated in each figure. The largest value of τ_e is 592, 305, and 392 ps for the apo, $(Cd^{2+})_1$, and $(Ca^{2+})_2$ states, respectively.

which are located in the middle of the loop forming the binding site, the average S^2 value of 0.63 for the apo state is increased to 0.87 in the $(Cd^{2+})_1$ state and 0.85 in the $(Ca^{2+})_2$ state. The slightly lower value of the average order parameter in the $(Ca^{2+})_2$ state than in the $(Cd^{2+})_1$ state is not significant (Table V). If the average S^2 values are interpreted by the diffusion in a cone model (eq 8), then the average θ_0 value of 31° in the apo state is reduced to 17° in the $(Cd^{2+})_1$ state and 19° in the $(Ca^{2+})_2$ state. Thus, in the absence of metal ion, the backbone amide groups in loop II exhibit relatively large amplitude fluctuations, which are substantially attenuated upon ligation of an ion. The model-free parameters for residues K55, N56, V61, and S62, which are located at the boundaries of the loop, are less strongly affected by ion binding. Since the Helmert contrasts for the mean model-free parameters for loop II (Table V) were performed using results for the entire loop (K55–S62), the *average* changes reflected in this analysis are attenuated by the influence of the residues at the loop boundaries.

Table III: Average Order Parameters and Average Internal Correlation Times As a Function of Structural Element and Ion Level of Calbindin D_{9k}[a]

structural element[b]	apo	$(Cd^{2+})_1$	$(Ca^{2+})_2$
	Average Order Parameter		
helix I	0.85 ± 0.01	0.85 ± 0.01	0.84 ± 0.01
loop I	0.80 ± 0.02	0.82 ● 0.01	0.82 ± 0.02
helix II	0.87 ± 0.01	0.880 ± 0.004	0.862 ± 0.004
helix III	0.82 ± 0.01	0.863 ± 0.005	0.838 ± 0.005
loop II	0.72 ± 0.04	0.86 ± 0.01	0.83 ± 0.01
helix IV	0.86 ± 0.01	0.84 ± 0.02	0.82 ± 0.02
	Average Internal Correlation Time (ps)		
helix I	22 ± 5	23 ± 5	23 ± 4
loop I	26 ± 5	10 ± 5	8 ± 4
helix II	11 ± 3	7 ± 2	3 ± 2
helix III	40 ± 4	19 ± 4	12 ± 2
loop II	75 ± 22	1 ± 1	5 ± 2
helix IV	18 ± 5	28 ± 9	26 ± 6

[a] Mean and standard error in the mean for elements of secondary structure for different levels of ion loading. Results for the linker loop are not shown. Residues for which relaxation parameters could not be measured in the $(Cd^{2+})_1$ state have not been included in the averages for the apo and $(Ca^{2+})_2$ states. All 15 pairwise comparisons of the mean order parameters (mean correlation times) for the different elements of secondary structure were performed for each ion level using Tukey's method for controlling the overall type I error at $\alpha = 0.05$. [b] The structural elements comprise the following residues (the number of residues are given in parentheses): helix I, E4–A14 (11); loop I, K16 and G18–Q22 (5); helix II, K25–E35 (11); helix III, L46–D54 (9); loop II, K55–S62 (8); helix IV, F63–I73 (11).

Table IV: Summary of Repeated-Measures Analysis of Variance of the Dependence of Order Parameters and Internal Correlation Times on the Number of Ions Bound and the Six Structural Elements of Calbindin D_{9k}[a]

		order parameter		internal correlation time	
effect tested	ν_1, ν_2	F statistic	p value	F statistic	p value
ion level	2, 48	46.05	0.0001	12.53	0.0001
structural element	5, 49	4.72	0.0014	2.59	0.0371
ion–structure interaction	10, 96	6.45	0.0001	4.60	0.0001
apo vs Cd1+Ca2	1, 49	13.38	0.0006	22.43	0.0001
Cd1 vs Ca2	1, 49	66.69	0.0001	1.90	0.1748

[a] The degrees of freedom, ν_1 and ν_2, and the F statistics and p values are given for the multivariate tests of the dependence of the model-free parameters on ion level and structural element. In each case, the null hypothesis is that the variable has no effect on the model-free parameters. The results are significant and the null hypothesis is rejected, if the p value is <0.05. The results for testing the null hypotheses that the values of contrast apo vs Cd1+Ca2 and contrast Cd1 vs Ca2 are equal to zero are also shown in the last two rows. The former compares the results for the apo state to the average results for the metal-bound states; the latter compares the results for the $(Cd^{2+})_1$ state to the results for the $(Ca^{2+})_2$ state. The contrasts are significantly different from zero (i.e., the results for the compared states are significantly different) if the p value is <0.05.

In contrast to loop II, the average order parameters for loop I are ~0.81 for three states of calbindin D_{9k}, which is rather close to the average for the four helices that make up the core of the protein. Furthermore, none of the individual order parameters for the residues in loop I are significantly different between any of the three states (Table I), and the Helmert contrasts for the mean model-free parameters of loop I are not significant (Table V). Consequently, the picosecond to nanosecond fluctuations of the backbone amide groups of this loop are found to be relatively restricted and independent of the level of ion ligation. Loop I has the S-100 type 14-residue sequence, including a proline at position 20, that distinguishes it from the loops found in consensus EF-hands; this difference

Table V: Pairwise *t*-Tests for Helmert Contrasts between Ion Levels for the Six Structural Elements of Calbindin D_{9k}[a]

structural element[b]	ν	critical value	order parameter: apo vs Cd1+Ca2	order parameter: Cd1 vs Ca2	internal correlation time: apo vs Cd1+Ca2	internal correlation time: Cd1 vs Ca2
helix I	10	3.716	1.04	4.77	−0.13	−0.02
loop I	4	5.951	−1.30	0.04	3.55	2.26
helix II	10	3.716	−0.79	7.95	1.64	1.75
helix III	8	3.991	−8.22	7.90	4.74	1.67
loop II	7	4.207	−3.14	4.08	3.05	−1.65
helix IV	10	3.716	3.14	3.97	−2.70	0.37

[a] The number of degrees of freedom (ν), the critical values for the paired *t*-tests, and the values of the test statistic for the various Helmert contrasts are listed for the six structural elements of the protein. Contrast apo vs $\overline{Cd1+Ca2}$ compares the results for the apo state to the average results for the metal-bound states; contrast Cd1 vs Ca2 compares the results for the $(Cd^{2+})_1$ state to the results for the $(Ca^{2+})_2$ state. Using the Bonferroni method, the critical values listed are for $\alpha = 0.002$, which controls the overall type I error to <0.05 for the 12 contrasts performed for the order parameters and for the internal correlation times. The contrasts are significant if the absolute value of the test statistic exceeds the critical value. [b] The structural elements comprise the following residues (the number of residues are given in parentheses): helix I, E4–A14 (11); loop I, K16 and G18–Q22 (5); helix II, K25–E35 (11); helix III, L46–D54 (9); loop II, K55–S62 (8); helix IV, F63–I73 (11).

apparently leads to a less flexible conformation in the absence of metal ions, as compared to the standard EF-hand. The lower flexibility of loop I may contribute to the lower affinity for cadmium ions of this site, as compared to loop II (Vogel et al., 1985; Akke et al., 1991).

Statistically significant effects in response to ion binding are observed on the model-free parameters of helices I–IV of calbindin D_{9k}, but these are much smaller than the effects on loop II. The most significant of these effects are that helix III becomes less flexible upon binding of the first ion to site II and that helices I–IV become slightly more flexible upon binding of the second ion (Table V). The average S^2 values can be interpreted by the diffusion in a cone model (eq 8); for example, the differences in the average order parameters for helix III (Table III) correspond to θ_0 values of 22°, 18°, and 20° for the apo, $(Cd^{2+})_1$, and $(Ca^{2+})_2$ states of the protein, respectively. Note that the statistical tests employed herein are sensitive to the number of residues included for a structural element. For example, the difference in order parameters for the $(Cd^{2+})_1$ and $(Ca^{2+})_2$ states is significant for helix IV but not for loop II (Table V), even though the actual value of the test statistic is smaller for helix IV than for loop II, because the larger number of residues for helix IV reduces the critical value for the statistical test. Additionally, the effects of ion ligation on the order parameters for the helices are small, and systematic errors that alter the order parameters between the three states cannot be entirely excluded. However, two observations suggest that the small differences observed in the relaxation data and corresponding model-free parameters are not artifacts: (i) values of the order parameters determined for the three states of the protein correspond closely for individual residues whose internal dynamics are not affected by ion binding, and (ii) the trends of the order parameters along the amino acid sequence are accurately reproduced for these residues. As an example of the latter observation, order parameters toward the middle of the helices tend to be larger in all three states of the protein [note an interesting parallel to the general trends in amide proton exchange rates of the helices (Skelton et al., 1992)].

One potential source of systematic error, differences in the final optimized overall correlation times for each state, was eliminated by recalculating the model-free parameters with the assumption that all three states of the protein have the same overall correlation time (data not shown). The results reported herein are unchanged. Relaxation measurements for the $^{13}C^{\alpha}$ spins are currently in progress in an effort to obtain additional experimental data to increase the reliability of the statistical analysis and confirm the trends observed in the ^{15}N data.

The model-free results for the linker loop region (F36–T45) of calbindin D_{9k} are very similar for the three states of the protein when data acquired at a single magnetic field are utilized. However, in the analysis of the $(Ca^{2+})_2$ state using relaxation data acquired at two magnetic fields (Kördel et al., 1992), the optimized model-free parameters are notably different from the results obtained using only the data acquired at 11.74 T. This observation suggests that ^{15}N relaxation for these residues is mediated by internal motions of the amide bond vectors with characteristic correlation times outside the extreme narrowing limit. Thus, a definitive assessment of the response of the linker loop dynamics to the binding of ions is not possible until a more complete characterization of the frequency dependence of the relaxation parameters is made.

In keeping with previous findings for $(Ca^{2+})_2$-calbindin D_{9k} (Kördel et al., 1992), amide groups in apo- and $(Cd^{2+})_1$-calbindin D_{9k} with low values of the order parameters generally exhibit rapid proton exchange with solvent, but residues with high values of S^2 exhibit a range of amide proton exchange rates. Hence, the three distinct categories (small S^2 and rapid exchange, large S^2 and rapid exchange, large S^2 and slow exchange) previously found in the $(Ca^{2+})_2$ state are equally applicable for the apo and $(Cd^{2+})_1$ states (Table I). Upon comparison of the cumulative results for all three states of the protein, both the ^{15}N relaxation and the amide exchange studies indicate greater flexibility in loop II, but less flexibility at the C-terminus, in the apoprotein than in the metal-bound states. However, this positive correlation between trends in the relaxation and the exchange data is not general, and some of the comparisons are rather surprising. For example, the average order parameter for loop I is indistinguishable in the three states, whereas the amide proton exchange rate constants for some of the residues in loop I are, in fact, *faster* in the $(Cd^{2+})_1$ state than in the apo state. The apparently higher rates of conformational exchange in the $(Cd^{2+})_1$ state detected by analysis of ^{15}N relaxation results (*vide infra*) may contribute to the faster rates of amide proton exchange with solvent observed for residues A15, K16, D19, and N21 in the $(Cd^{2+})_1$ state as compared to the apo state (Skelton et al., 1992a).

In summary, the comparisons between the relaxation and exchange results for the various structural elements of calbindin D_{9k} indicate that changes in the internal dynamics in response to ion binding occur over a wide range of time scales, that the changes at different time scales are not necessarily correlated, and that the exact nature of the changes is different for the various structural elements of the protein.

Conformational Exchange. The exchange contribution (R_{ex}) to the transverse relaxation is caused by processes that dephase transverse magnetization during the CPMG sequence (Bloom et al., 1965). Thus, for such effects to be noticeable, the rate of exchange must be on the order of the inverse of the time between the refocusing pulse and the formation of the spin–echo, i.e., for a delay between refocusing pulses (ξ) of 1 ms, the rate must be comparable to $2/\xi = 2000\ s^{-1}$. Substantial R_{ex} terms were obtained in the model-free optimization for residues A14, K16, G18, D19, and Q22 in loop I (the unoccupied ion-binding site) of the $(Cd^{2+})_1$ state.

In principle, the R_{ex} terms could arise either from chemical exchange between the $(Cd^{2+})_1$ state and the small amount of the $(Cd^{2+})_2$ state present at equilibrium or from exchange between distinct conformers of the $(Cd^{2+})_1$ state. The chemical reaction for exchange between the $(Cd^{2+})_1$ and $(Cd^{2+})_2$ states is given by

$$(Cd^{2+})_1 + Cd^{2+} \underset{k_{off}}{\overset{k_{on}}{\rightleftarrows}} (Cd^{2+})_2 \qquad (9)$$

and the rate of exchange is given by

$$r_{ex} = k_{off} + k_{on}[Cd^{2+}] = k_{off} + \beta k_{off} \qquad (10)$$

where $\beta = [(Cd^{2+})_2]/[(Cd^{2+})_1]$; $[Cd^{2+}]$, $[(Cd^{2+})_1]$, and $[(Cd^{2+})_2]$ are the concentrations of the free cadmium ions, the $(Cd^{2+})_1$ state, and the $(Cd^{2+})_2$ state, respectively. The ratio β is estimated to be less than 0.05 under the conditions used here, from an analysis of ^{15}N chemical shifts during titration from the $(Cd^{2+})_1$ state to the $(Cd^{2+})_2$ state (M. Akke, G. Carlström, & W. J. Chazin, unpublished results). Using the value $k_{off} = 700\ s^{-1}$, as determined from ^{113}Cd NMR (Vogel et al., 1985), and eq 10, r_{ex} must be $<2000\ s^{-1}$. Thus, the process given by eq 9 should not contribute to the R_{ex} terms.

The possibility of a chemical exchange effect on R_2 can be further addressed by considering the contribution to the decay rate constant for an ^{15}N spin in a CPMG sequence due to fast exchange between the $(Cd^{2+})_1$ and $(Cd^{2+})_2$ states, given by (Luz & Meiboom, 1963)

$$R_{ex} = r_{ex}^{-1}\left[1 - \frac{2}{\xi r_{ex}}\tanh\left(\frac{\xi r_{ex}}{2}\right)\right]\frac{\beta\omega_{ex}^2}{(1+\beta)^2} \qquad (11)$$

where r_{ex} is defined by eq 10, $\omega_{ex}^2 = [\omega(Cd^{2+})_2 - \omega(Cd^{2+})_1]^2$, and $\omega(Cd^{2+})_2$ and $\omega(Cd^{2+})_1$ are the Larmor frequencies of the spin in the $(Cd^{2+})_1$ and $(Cd^{2+})_2$ states, respectively. As seen from eq 11, R_{ex} is linear in ω_{ex}^2 for a given value of r_{ex}; however, the data pairs formed by R_{ex} and ω_{ex}^2 for the residues that have values of R_{ex} greater than $1\ s^{-1}$ in the $(Cd^{2+})_1$ state do not show a linear relationship (correlation coefficient of 0.07; data not shown).

Together, these two lines of reasoning strongly imply that the R_{ex} terms are not due to a chemical exchange process between the $(Cd^{2+})_1$ state and a small equilibrium population of the $(Cd^{2+})_2$ state, but rather are due to conformational exchange between distinct conformations of the protein in the $(Cd^{2+})_1$ state. Further kinetic analysis is not possible, since the chemical shifts of the discrete $(Cd^{2+})_1$ substates cannot be determined.

Exchange contributions to the transverse relaxation rate constant are also observed in the apo state of the protein. The possibility that this contribution is due to chemical exchange between the apo state and the small equilibrium population of the $(Ca^{2+})_2$ state can be excluded following the same line of reasoning as that provided above for the $(Cd^{2+})_1$ state. The amount of contaminating $(Ca^{2+})_2$ states in the apoprotein sample used for the relaxation measurements is estimated to be less than 0.5%, since cross-peaks from the $(Ca^{2+})_2$ state could not be detected in the 2D ^1H–^{15}N spectra. Since the value of k_{off} for Ca^{2+} is $<20\ s^{-1}$ (Vogel et al., 1985), the exchange contribution observed in the apo state can also be attributed to intrinsic conformational heterogeneity.

One likely interpretation of the higher *apparent* rates of conformational exchange in the $(Cd^{2+})_1$ state versus the apo state of calbindin D_{9k} (Table I) is that the conformational substates of loop I are sampled more frequently in the $(Cd^{2+})_1$ state than in the apo state. Although the high-frequency dynamics characterized by the model-free parameters implies that loop I is rather rigid, the exchange contributions characterized by R_{ex} indicate that there is considerably greater flexibility on the slower time scale. The interconversion between conformational states occurring on the slower time scale may, in fact, play an important functional role in calbindin D_{9k}, serving to facilitate binding of ions to loop I.

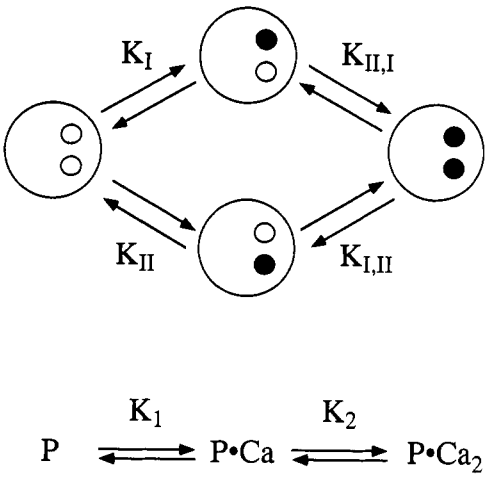

FIGURE 5: Schematic diagram of the calcium-binding process in calbindin D_{9k}, defining the site-specific (microscopic) binding constants (K_I, K_{II}, $K_{I,II}$, and $K_{II,I}$) and the stoichiometric (macroscopic) binding constants (K_1 and K_2). For clarity, the free calcium ions have been omitted in the figure.

Conformational exchange processes that occur on time scales slower than the overall rotational correlation time have also been observed in NMR spin relaxation studies of proteins [e.g., Kay et al. (1989), Clore et al. (1990), Palmer et al. (1991a), Stone et al. (1992), and Barbato et al. (1992)]. Of particular relevance to the present study are that anomalously large ^{15}N R_2 values probably associated with conformational exchange were observed in the calcium-loaded state of calmodulin for residues in or neighboring the first ion-binding loop of each of the two globular domains (Barbato et al., 1992) and that conformational exchange with a rate of $\sim 10^4$–$10^5\ s^{-1}$ in the N-terminal calcium-binding sites of calmodulin and troponin C has been inferred from ^{113}Cd NMR (Forsén et al., 1986). In contrast, no significant conformational exchange contributions to ^{15}N R_2 values were identified for calcium-loaded calbindin D_{9k}, even though substantial R_{ex} terms have been detected for the apo and $(Cd^{2+})_1$ states of the protein. The variation in conformational exchange observed for the three states of calbindin D_{9k} is attributed to fundamental differences between apo, half-loaded, and fully loaded calcium-binding domains. Further studies are required to establish whether the apparent differences between calcium-loaded calmodulin, troponin C, and calbindin D_{9k} reflect characteristic differences between consensus (calmodulin-like) and S-100-like globular calcium-binding domains.

Cooperativity in Calcium Binding and Fast Time Scale Fluctuations. The cooperative binding of calcium ions to bovine calbindin D_{9k} has been firmly established (Linse et al., 1987, 1991). Figure 5 shows a schematic diagram of the ion-binding processes and defines the site-specific (microscopic) binding constants, K_I, K_{II}, $K_{I,II}$, $K_{II,I}$, and the stoichiometric (macroscopic) binding constants, K_1 and K_2. Positive cooperativity is defined as $\Delta\Delta G = \Delta G_{II,I} - \Delta G_{II} = \Delta G_{I,II} - \Delta G_I < 0$, where the relevant processes can be identified by the indices of the corresponding binding constants in Figure 5. Thus, positive cooperativity entails higher affinity for an ion to site II in the presence of an ion in site I than when site

I is unoccupied, and vice versa. In calbindin D_{9k}, the two site binding constants, K_I and K_{II}, are nearly equal, $1 < K_{II}/K_I < 3$, and $K_2 > K_1$ (Linse et al., 1987, 1991). These two observations imply positive cooperativity. In addition, they imply the following additional aspect of cooperativity: $\Delta G_{II,I} - \Delta G_I < 0$ and $\Delta G_{I,II} - \Delta G_{II} < 0$, i.e., in a stepwise binding pathway, the affinity for the second ion is higher than that for the first ion. Note that, in the case of a symmetric system with identical sites (where $\Delta G_{II} = \Delta G_I$), this latter condition is equivalent to positive cooperativity, e.g., $\Delta G_{I,II} - \Delta G_{II} = \Delta G_{I,II} - \Delta G_I < 0$.

Since calbindin D_{9k} is asymmetric, comparison between the three states [e.g., apo, $(Cd^{2+})_1$, and $(Ca^{2+})_2$] cannot fully address the molecular basis for cooperativity [without making the simplifying assumption of near-identical sites (Akke et al., 1991)],[4] but it can address the *cooperative phenomenon*, $\Delta G_{I,II} - \Delta G_{II} < 0$, for the apo $\rightarrow$ $(Ca^{2+})_1 \rightarrow (Ca^{2+})_2$ pathway. Since low-order parameters in these systems imply high flexibility and vice versa, differences in order parameters between different states can be qualitatively interpreted in terms of entropy changes arising from the fast time scale fluctuations. A qualitative view of possible entropic contributions to the cooperative phenomenon $\Delta G_{I,II} - \Delta G_{II} < 0$ can thus be obtained by noting the differences in the values of the order parameters between the $(Cd^{2+})_1$ and apo states (corresponding to an entropic contribution to ΔG_{II}) and between the $(Ca^{2+})_2$ and $(Cd^{2+})_1$ states (corresponding to an entropic contribution to $\Delta G_{I,II}$). The present data exhibit large differences in the order parameters for residues G57, D58, G59, and E60 in loop II (and to a lesser extent for S74 and Q75 at the C-terminus) between the apo state on one hand and the $(Cd^{2+})_1$ and $(Ca^{2+})_2$ states on the other; in addition, the rigidity of helices II–IV appears to depend upon the number of ions bound. The increased conformational restriction of the N–H bond vectors for G57, D58, G59, E60, and helix III in the $(Cd^{2+})_1$ state compared to the apo state provides an unfavorable entropic contribution to ΔG_{II}. The decreased conformational restriction of the N–H bond vectors for helices II–IV in the $(Ca^{2+})_2$ state compared to the $(Cd^{2+})_1$ state provides a small favorable contribution to $\Delta G_{I,II}$. The overall result is a negative entropic contribution to the cooperative phenomenon, $\Delta G_{I,II} - \Delta G_{II} < 0$, which would act to increase the affinity for the second ion to site I in relation to the affinity for the first ion to site II.

The results obtained here identify changes in internal motions of the backbone N–H bond vectors on the picosecond to nanosecond time scale that are associated with entropic contributions to the total free energy of the cooperative phenomenon $\Delta G_{I,II} - \Delta G_{II} < 0$. However, the relative importance of the entropic contributions from the picosecond to nanosecond fluctuations of the N–H bond vectors cannot be assessed quantitatively at present because other effects undoubtedly contribute to cooperativity. For example, both the conformational exchange contributions to the transverse relaxation rate constant observed herein and the amide proton exchange measurements (Skelton et al., 1992b) indicate that fluctuations occurring on different time scales are also influenced by ion binding.

[4] Recent studies by Carlström and Chazin (1993) suggest that calbindin D_{9k} is highly asymmetric in its conformational–dynamical response to calcium binding, even though the site binding constants K_I and K_{II} are nearly equal. Therefore, to address the molecular basis for cooperativity, the apo, $(Ca^{2+})_1^I$, $(Ca^{2+})_1^{II}$, and $(Ca^{2+})_2$ states of calbindin D_{9k} must all be compared because the two binding sites are not identical.

CONCLUDING REMARKS

In order to determine the changes in intramolecular dynamics that accompany binding of ions to calbindin D_{9k}, the previously reported ^{15}N spin relaxation measurements performed on the $(Ca^{2+})_2$ state (Kördel et al., 1992) have been extended to the apo and $(Cd^{2+})_1$ states of the protein. The ^{15}N relaxation data have been analyzed using the extended Lipari–Szabo model-free formalism to determine order parameters and effective internal correlation times for the backbone N–H bond vectors. The backbone dynamics of the four helices are similar, and the responses to ion binding are variable but consistently small in magnitude. Helix III, which is located between the linker loop and binding site II, is the helix most strongly affected by ion binding; intramolecular fluctuations decrease slightly upon binding of the first ion and then increase slightly upon binding of the second. In contrast to the helices, the backbone dynamics of the two binding loops are dramatically different: in the apo state, loop I has substantially smaller fluctuations on the picosecond to nanosecond time scale than loop II, and the effect of ion binding on these fluctuations is substantially smaller in loop I than in loop II. Interestingly, a strong asymmetry in the response of the two EF-hands to ion binding is also found by comparing the three-dimensional structures of the three states of the protein (Kördel et al., 1993 and unpublished results). The substantial difference in the (fast time scale) dynamical responses to the binding of ions in loop I and loop II was not expected and suggests that fundamental differences exist between consensus-type EF-hand calcium-binding sites and the N-terminal binding sites found in S-100 and calbindin D_{9k}. Clearly, such differences provide a means for modulating the binding properties of EF-hand calcium-binding proteins. However, comments on the functional significance of these properties would be premature at this time, since only a limited database is available.

A detailed understanding of protein function requires characterization of the structure and dynamical properties of the protein. Obtaining experimental information on internal degrees of freedom over a wide range of time scales in proteins presents a formidable experimental challenge; complete characterization is not likely to be achieved in the foreseeable future for any protein. The present results provide qualitative evidence for entropic contributions to the cooperativity in ion binding by calbindin D_{9k} that arise from changes in the fast time scale fluctuations of the backbone N–H bond vectors. The substantial asymmetry in the dynamical response of the two sites to ion binding is a novel observation for the family of EF-hand calcium-binding proteins and suggests a level of complexity in the global binding process of calbindin D_{9k} that can only be addressed by further studies of half-saturated states of the protein.

ACKNOWLEDGMENT

We gratefully acknowledge Professor Sture Forsén for his encouragement and helpful insights, Dr. Mark Rance for continued assistance with experimental techniques, Eva Thulin for protein expression and purification, and Drs. Rafael Brüschweiler, Göran Carlström, and Martin Stone for stimulating discussions.

SUPPLEMENTARY MATERIAL AVAILABLE

A table containing the measured values of R_1, R_2, and NOE for each residue of calbindin D_{9k} in the apo and $(Cd^{2+})_1$ states (4 pages). Ordering information is given on any current masthead page.

REFERENCES

Abragam, A. (1961) *The Principles of Nuclear Magnetic Resonance*, Clarendon Press, Oxford, England.

Akke, M., Forsén, S., & Chazin, W. J. (1991) *J. Mol. Biol. 220*, 173–189.

Akke, M., Drakenberg, T., & Chazin, W. J. (1992) *Biochemistry 31*, 1011–1020.

Barbato, G., Ikura, M., Kay, L. E., Pastor, R. W., & Bax, A. (1992) *Biochemistry 31*, 5269–5278.

Barkhuijsen, H., Beer, R. J., & Van Ormondt, D. (1987) *J. Magn. Reson. 73*, 553–557.

Bax, A., Sparks, S. W., & Torchia, D. A. (1989) *Methods Enzymol. 176*, 134–150.

Bloom, M., Reeves, L. W., & Wells, E. J. (1965) *J. Chem. Phys. 42*, 1615–1624.

Boyd, J., Hommel, U., & Campbell, I. D. (1990) *Chem. Phys. Lett. 175*, 477–482.

Burum, D. P., & Ernst, R. R. (1980) *J. Magn. Reson. 39*, 163–168.

Carlström, G., & Chazin, W. J. (1993) *J. Mol. Biol. 231*, 415–430.

Carr, H. Y., & Purcell, E. M. (1954) *Phys. Rev. 94*, 630–638.

Chazin, W. J., Kördel, J., Drakenberg, T., Thulin, E., Brodin, P., Grundström, T., & Forsén, S. (1989a) *Proc. Natl. Acad. Sci. U.S.A. 86*, 2195–2198.

Chazin, W. J., Kördel, J., Drakenberg, T., Thulin, E., Hofmann, T., & Forsén, S. (1989b) *Biochemistry 28*, 8646–8653.

Christakos, S., Gabrielides, C., & Rhoten, W. B. (1989) *Endocrinol. Rev. 10*, 3–26.

Clore, M. G., Driscoll, P. C., Wingfield, P. T., & Gronenborn, A. M. (1990a) *Biochemistry 29*, 7387–7401.

Clore, M. G., Szabo, A., Bax, A., Kay, L. E., Driscoll, P. C., & Gronenborn, A. M. (1990b) *J. Am. Chem. Soc. 112*, 4989–4991.

Cole, J. W. L., & Grizzle, J. E. (1966) *Biometrics 22*, 810–828.

Delsuc, M. A., & Lallemand, J. Y. (1986) *J. Magn. Reson. 69*, 504–507.

Devore, J. L. (1982) *Probability and Statistics for Engineering and the Sciences*, Brooks/Cole, Monterey, CA.

Forsén, S., Vogel, H., & Drakenberg, T. (1986) in *Calcium and Cell Function* (Cheung, W. Y., Ed.) Vol. 6, pp 113–157, Academic Press, New York.

Halle, B., & Wennerström, H. (1981) *J. Chem. Phys. 75*, 1928–1943.

Heizmann, C. W., & Hunziker, W. (1991) *Trends Biol. Sci. 16*, 98–103.

Hiyama, Y., Niu, C.-H., Silverton, J. V., Bavoso, A., & Torchia, D. A. (1988) *J. Am. Chem. Soc. 110*, 2378–2383.

James, P., Vorherr, T., Thulin, E., Forsén, S., & Carafoli, E. (1991) *FEBS Lett. 278*, 155–159.

Kay, L. E., Torchia, D. A., & Bax, A. (1989) *Biochemistry 28*, 8972–8979.

Kay, L. E., Nicholson, L. K., Delaglio, F., Bax, A., & Torchia, D. A. (1992) *J. Magn. Reson. 97*, 359–375.

Kraulis, P. (1991) *J. Appl. Crystallogr. 24*, 946–950.

Kretsinger, R. H. (1972) *Nature New Biol. 240*, 85–88.

Kördel, J., Forsén, S., & Chazin, W. J. (1989) *Biochemistry 28*, 7065–7074.

Kördel, J., Forsén, S., Drakenberg, T., & Chazin, W. J. (1990) *Biochemistry 29*, 4400–4409.

Kördel, J., Skelton, N. J., Akke, M., Palmer, A. G., III, & Chazin, W. J. (1992) *Biochemistry 31*, 4856–4866.

Kördel, J., Skelton, N. J., Akke, M., & Chazin, W. J. (1993) *J. Mol. Biol. 231*, 711–734.

Linse, S., Brodin, P., Drakenberg, T., Thulin, E., Sellers, P., Elmdén, K., Grundström, T., & Forsén, S. (1987) *Biochemistry 26*, 6723–6735.

Linse, S., Johansson, C., Brodin, P., Grundström, T., Drakenberg, T., & Forsén, S. (1991) *Biochemistry 30*, 154–162.

Lipari, G., & Szabo, A. (1980) *Biophys. J. 30*, 489–506.

Lipari, G., & Szabo, A. (1981) *J. Chem. Phys. 75*, 2971–2976.

Lipari, G., & Szabo, A. (1982a) *J. Am. Chem. Soc. 104*, 4546–4559.

Lipari, G., & Szabo, A. (1982b) *J. Am. Chem. Soc. 104*, 4559–4570.

Luz, Z., & Meiboom, S. (1963) *J. Chem. Phys. 39*, 366–370.

Marion, D., & Wüthrich, K. (1983) *Biochem. Biophys. Res. Commun. 113*, 967–974.

Marion, D., Ikura, M., & Bax, A. (1989) *J. Magn. Reson. 84*, 425–430.

Meiboom, S., & Gill, D. (1958) *Rev. Sci. Instrum. 29*, 688–691.

Messerle, B. A., Wider, G., Otting, G., Weber, C., & Wüthrich, K. (1989) *J. Magn. Reson. 85*, 608–613.

Morris, G. A., & Freeman, R. (1979) *J. Am. Chem. Soc. 101*, 760–762.

Nirmala, N. R., & Wagner, G. (1988) *J. Am. Chem. Soc. 110*, 7557–7558.

Otting, G., & Wüthrich, K. (1988) *J. Magn. Reson. 76*, 569–574.

Otting, G., Widmer, H., Wagner, G., & Wüthrich, K. (1986) *J. Magn. Reson. 66*, 187–193.

Palmer, A. G., III, Rance, M., & Wright, P. E. (1991a) *J. Am. Chem. Soc. 113*, 4371–4380.

Palmer, A. G., III, Cavanagh, J., Wright, P. E., & Rance, M. (1991b) *J. Magn. Reson. 93*, 151–170.

Palmer, A. G., III, Skelton, N. J., Chazin, W. J., Wright, P. E., & Rance, M. (1992) *Mol. Phys. 75*, 699–711.

Peng, J., & Wagner, G. (1992a) *Biochemistry 31*, 8571–8586.

Peng, J., & Wagner, G. (1992b) *J. Magn. Reson. 98*, 308–332.

Press, W. H., Flannery, B. P., Teukolsky, S. A., & Vetterling, W. T. (1986) *Numerical Recipes*, Cambridge University Press, Cambridge, UK.

Seamon, K. B., & Kretsinger, R. H. (1983) *Met. Ions. Biol. 6*, 1–51.

Shaka, A. J., Keeler, J., Frenkiel, T., & Freeman, R. (1983) *J. Magn. Reson. 52*, 334–338.

Shaka, A. J., Barker, P. B., & Freeman, R. (1985) *J. Magn. Reson. 64*, 547–552.

Shoji, A., Ozaki, T., Fujito, T., Deguchi, K., Ando, S., & Ando, I. (1989) *Macromolecules 20*, 2860–2863.

Shoji, A., Ozaki, T., Fujito, T., Deguchi, K., Ando, S., & Ando, I. (1990) *J. Am. Chem. Soc. 112*, 4693–4697.

Skelton, N. J., Kördel, J., Forsén, S., & Chazin, W. J. (1990) *J. Mol. Biol. 213*, 593–598.

Skelton, N. J., Kördel, J., Akke, M., & Chazin, W. J. (1992a) *J. Mol. Biol. 227*, 1100–1117.

Skelton, N. J., Akke, M., Kördel, J., Thulin, E., Forsen, S., & Chazin, W. J. (1992b) *FEBS Lett. 303*, 136–140.

Skelton, N. J., Palmer, A. G., III, Akke, M., Kördel, J., & Chazin, W. J. (1993) *J. Magn. Reson.* (in press).

Staun, M. (1991) *Dan. Med. Bull. 38*, 271–282.

Stone, M. J., Fairbrother, W. J., Palmer, A. G., III, Reizer, J., Saier, M., Jr., & Wright, P. E. (1992) *Biochemistry 31*, 4394–4406.

Szebenyi, D. M. E., & Moffat, K. (1986) *J. Biol. Chem. 261*, 8761–8777.

Vogel, H. J., Drakenberg, T., Forsén, S., O'Neil, J. D. J., & Hofmann, T. (1985) *Biochemistry 24*, 3870–3876.

Vold, R. R., & Vold, R. L. (1976) *J. Chem. Phys. 64*, 320–332.

Wennerström, H., Lindman, B., Söderman, O., Drakenberg, T., & Rosenholm, J. B. (1979) *J. Am. Chem. Soc. 101*, 6860–6864.

Winer, B. J. (1991) *Statistical Principles of Experimental Design*, 3rd ed., McGraw-Hill, New York.